ACS Photonics

Article

pubs.acs.org/journal/apchd5

Optical-Electronic Analysis of the Intrinsic Behaviors of Nanostructured Ultrathin Crystalline Silicon Solar Cells

Ilker Karakasoglu,[†] Ken Xingze Wang,[‡] and Shanhui Fan*,[†]

[†]Department of Electrical Engineering, and [‡]Department of Applied Physics, Stanford University, Stanford, California 94305, United States

ABSTRACT: Light trapping and antireflection via nanotexturing are prominent methods for improved efficiency in solar cells. We present a combined three-dimensional optical and electronic simulation to calculate the intrinsic limits on the efficiency in ultrathin nanotextured crystalline silicon solar cells. Our simulation incorporates the fundamental loss mechanisms including Auger recombination and surface recombination. The simulation shows that an optimized 3 μm thick structure with double-sided nanocone gratings yields an efficiency of 24.9% with a short-circuit current density of 36.6 mA/cm^2 and an open-circuit voltage of 0.79 V. We also introduce an analytic model that describes the electronic properties. This model significantly simplifies the optical-electronic analysis of nanostructured solar cells.

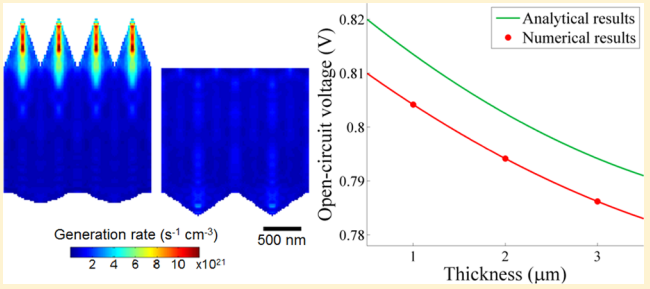

KEYWORDS: *thin-film solar cells, nanostructuring, light trapping, antireflection, crystalline silicon, open-circuit voltage*

Nanostructured designs, utilized for crystalline silicon (c-Si) solar cells, have been shown to achieve broadband light absorption enhancement as compared to flat cells.[1−7] Such absorption enhancement can be directly expressed as the increase of the photocurrent. However, in order to understand how nanostructuring influences the efficiency, one would also need to evaluate how the voltage is affected. Especially, a major concern with nanostructured solar cells is that the nanostructuring introduces more surface area, which causes surface recombination losses. Therefore, combining optical and electrical analyses is becoming important in nanostructured solar cell design in order to evaluate the performance. Previous integrated optical and electrical analyses, involving electrical simulations of specific junction configurations used in the cell, provided important insights about the performance of specific solar cell devices.[8−11] For further improvement of solar cell efficiency, however, it is important to also understand the performance limit of a given structure, assuming only the fundamental recombination mechanisms of the material.

In this paper, we undertake an alternative combined electrical and optical analysis of nanostructured solar cells. Instead of considering specific junction configurations, we aim to compute, for a given nanostructured cell, an upper theoretical bound on its efficiency, taking into account both its optical properties and the recombination properties such as Auger recombination and surface recombination from the perspective of detailed balance. Such an efficiency bound can be reached if both the junctions and the contacts are assumed to be ideal. We discuss the numerical procedure of this analysis, using a double-sided nanocone structure as an example. As a key result of the paper, we also show that the electronic aspects of the solar cell and, in particular, the increase of surface recombination due to nanopatterning can be well accounted for by a simple analytic model. The combination of the numerical and analytic results allows us to quantitatively discern the recombination losses on the performance of the nanostructured solar cells.

We start by providing a brief summary of the analysis procedure. We treat a given nanostructured solar cell in its entirety as the active region. The photocurrent of the cell is computed by the absorption in it. The open-circuit voltage is directly expressed as a function of excess carrier densities in the presence of sunlight:[12]

$$V_{OC} = \frac{kT}{q}\ln\left(\frac{\Delta n \times (\Delta p + N_A)}{n_i^2} + 1\right) \quad (1)$$

where Δn and Δp are excess steady-state electron and hole concentrations, respectively, N_A is the doping concentration of the active region, n_i is the intrinsic carrier concentration, k is the Boltzmann constant, T is the temperature, and q is the elementary charge. In all our calculations, we consider cells operating at the ambient temperature T = 300 K, where n_i = 1.45 × 10^{10} cm^{-3}. To use eq 1, one needs to assume that the carrier concentrations are uniform in space, which as we will see in the simulation is indeed the case for our system. Having computed the photocurrent and the open-circuit voltage, we deduce the energy conversion efficiency with a detailed-balance analysis.

Our analysis intentionally assumes ideal junctions and contacts and does not include a detailed model of the junctions and contacts. Here we explicitly state some of the main

Received: February 22, 2015
Published: June 15, 2015

DOI: 10.1021/acsphotonics.5b00081
ACS Photonics 2015, 2, 883−889

nonidealities that we ignore in our analysis: We have assumed that the active area constitutes the whole cell. For carrier extraction purposes practical solar cells have heavily doped p and n regions, which have additional recombinations that we do not consider here. Also, we have ignored the Shockley–Read–Hall recombination. The numerical results obtained therefore represent an upper bound of what one might obtain in practical solar cells with the same optical structures. However, the approach here is well justified since our aim here is to understand the fundamental limit of a given structure subject to recombination. From a fundamental physics perspective, as Green emphasized, the junction field is just incidental for the operation of a p–n junction solar cell.[13] The main driving force of charge separation is the excess amount of chemical potential of charge carriers. P–n junctions merely introduce selective contacts: n-type region for the conduction band and p-type region for the valence band. From a practical experimental perspective, the measurement of light-induced carrier densities in a wafer before junctions or contacts are introduced has been widely used to predict and assess the performance of the solar cells that will be made with the same wafer.[14] Our approach here is motivated by the theoretical consideration in refs 12 and 13 and is directly relevant for the class of experiments as described in ref 14 that can be performed on nanophotonic solar cells.

While our analysis is applicable to all nanostructured solar cells, to illustrate it, we use double-sided nanocone gratings as an example model structure (Figure 1) for their superior light-trapping properties.[15] The structure is composed of a textured c-Si film with circular nanocones on its front and back surfaces. We define the thickness of a flat film structure that contains the same amount of silicon as the *equivalent thickness* of the nanostructured film. The film stands on a perfect electric conductor (PEC) mirror, which is a simple approximation of a silver back-reflector.[16] Such a structure has been shown to achieve light absorption and photocurrent close to the Yablonovitch limit.[16] The whole film is assumed to have light p-type uniform doping.

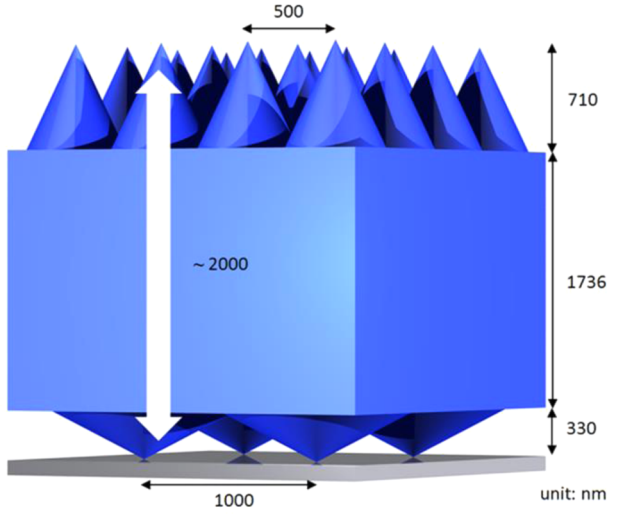

Figure 1. Three-dimensional model of a studied solar cell. The blue region represents the silicon, and the gray region represents a reflecting mirror made of a perfect electrical conductor. The geometry is optimized to maximize light absorption according to ref 16. The equivalent thickness of the structure is 2 μm. The physical thickness of the structure is 2.776 μm.

We first present the numerical analysis, which comprises two parts: optical and electrical. We start with the optical simulations. Rigorous coupled wave analysis (RCWA)[17−19] is used to obtain three-dimensional data of the absorbed light's electric field intensity. The structure is excited for the wavelengths in the solar spectrum where Si is optically absorbing (290–1100 nm).[20] The electric field intensity profile at each incident wavelength can be converted into a wavelength-dependent photocarrier generation rate:

$$G(\lambda) = \frac{\varepsilon(\lambda)''|E(\lambda)|^2}{2\hbar} \tag{2}$$

where ε'' is the imaginary part of the permittivity, E is the electric field, and $\hbar$ is the reduced Planck constant. After weighing the incident irradiance at each wavelength assuming the air mass 1.5 (AM1.5) solar spectrum, we obtain the carrier generation rate profiles integrated over the whole solar spectrum as shown in Figure 2.

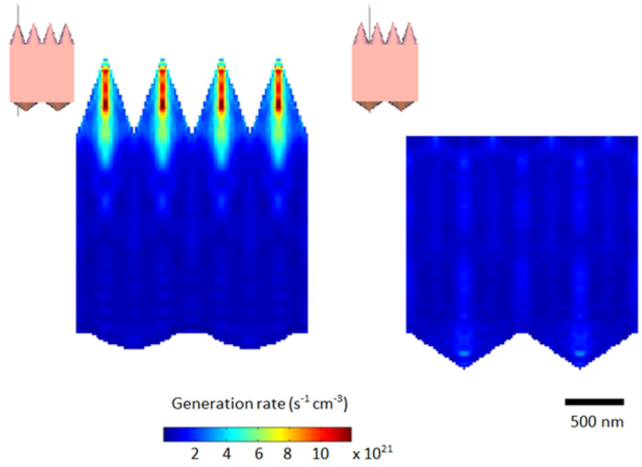

Figure 2. 2D cross sections of carrier generation rates obtained from 3D RCWA simulations. Insets show where the cross sections are taken. Light is normally incident upon the structure. To simulate the effect of an unpolarized source, both polarizations are simulated, and then the generation rates are averaged. Texturing changes both the amount of light absorbed and where it is localized. The carrier generation rate is strongly localized near the front cones.

The generation rate determined from the optical simulations is then used as the input source term in the electrical simulations, in order to determine the steady-state carrier concentration distributions. The electrical simulations are performed in 3D. We use a commercial software package (Sentaurus TCAD)[21] to solve the drift-diffusion model for carrier dynamics, which is defined by Poisson and continuity equations:

$$\nabla^2\psi = -\frac{q}{\varepsilon}(p - n - N_A) \tag{3.a}$$

$$\nabla J_n = -\nabla J_p = q(R - G) \tag{3.b}$$

$$J_n = qD_n\nabla n - q\mu_n n\nabla\psi \tag{3.c}$$

$$J_p = -qD_p\nabla p - q\mu_p p\nabla\psi \tag{3.d}$$

DOI: 10.1021/acsphotonics.5b00081
ACS Photonics 2015, 2, 883–889

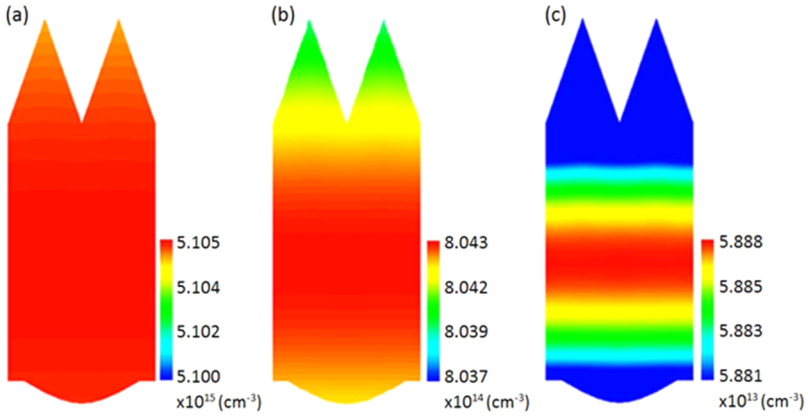

Figure 3. 2D cross sections of steady-state minority carrier (electron) distributions for three surface recombination velocities: (a) 20 cm/s, (b) 100 cm/s, and (c) 1000 cm/s. The equivalent thickness is kept constant at 2 μm. In the simulation we observe uniform steady-state carrier distributions, in spite of significant nonuniformity of the carrier generation profiles. In general, one can define an effective minority carrier diffusion length given by $L = (D\tau_{\text{eff}})^{1/2}$, where τ_{eff} is the effective lifetime. As long as the structure has a thickness $W \ll L$, the carrier distribution will be uniform. By the same argument, the carrier distribution will remain uniform also in the presence of surface recombination. The surface recombination will reduce minority carrier lifetime and hence reduce the effective minority carrier diffusion length. However, as long as the condition $W \ll L$ is satisfied, the carrier distribution will remain uniform.

where ψ is the electrostatic potential, q is the elementary electronic charge, ε is the dielectric function, n and p are the electron and hole concentrations, N_A is the doping concentration, R is the overall recombination rate, which includes bulk and surface recombination rates, G is the generation rate obtained from the optical simulations, and J_i, D_i, and μ_i are the current densities, diffusion coefficients, and mobilities; i = n, p. Bulk recombination lifetime (measured in s) is given by[22]

$$\tau_{\text{bulk}} = \frac{\Delta n}{np(C_n n_0^{0.65} + C_p p_0^{0.65} + C_a \Delta n^{0.8} + B)} \tag{4}$$

with the constants $C_n = 1.8 \times 10^{-24}$, $C_p = 6 \times 10^{-25}$, $C_a = 3 \times 10^{-27}$, and $B = 9.5 \times 10^{-15}$. Δn is the excess electron concentration; n_0 and p_0 are the thermal equilibrium concentrations of electrons and holes. All carrier concentrations in eq 4 are in units of cm^{-3}. Since we work only with a p-doped film, a single bulk lifetime is used with minority carriers being electrons. Auger recombination is the dominant bulk loss mechanism in c-Si cells. While the radiative recombination is accounted for with the term B in eq 4, it is weak except for very high carrier injection levels.[22] Another bulk recombination process, (defect -assisted) Shockley–Read–Hall (SRH) recombination, is initially assumed to be negligible. Unlike Auger and radiative recombinations, SRH recombination can be eliminated in principle with the eradication of defects. Even with the inclusion of SRH recombination, Auger recombination has been found to be the dominant bulk recombination process for carrier densities higher than 10^{15}cm^{-3} (high-injection regime).[23,24] Our numerical and analytic models indicate that carrier densities stay at the high-injection level except for very high surface recombination velocities (>100 cm/s). We also find that for those high surface recombination velocities, surface recombination dominates over total bulk recombination. Therefore, it is also safe to assume that SRH recombination is negligible. Nonetheless, at the end of this paper we show the dependency of the open-circuit voltage and the efficiency on SRH recombination.

Surface recombination is numerically modeled by the current density loss:

$$J_{\text{Surface}} = q\delta n S_e \tag{5}$$

where δn is the excess minority carrier concentration at the surface and S_e is the surface recombination velocity.

In our simulations, we vary the surface recombination velocity from 2000 cm/s down to 1 cm/s. The simulation results indicate a nearly uniform steady-state carrier distribution for all values in this range. Three of such carrier distributions are shown in Figure 3 for surface recombination velocities of 20, 100, and 1000 cm/s. In the most extreme case with a surface recombination velocity of 2000 cm/s, the difference between highest and lowest concentrations throughout the cell is below 0.2% of the average number of carriers. An unpassivated surface can typically have a surface recombination velocity as high as 2000 cm/s, while extremely low surface recombination velocities below 2 cm/s have been achieved.[25,26] Hence, our simulations show that the steady-state carrier densities are near uniform for all practical values of surface recombination velocity values.

Using the numerical analysis procedure as outlined above, we can now determine the efficiency of such nanophotonic solar cells. The open-circuit voltage of the cell is calculated using eq 1 since the carrier density is uniform. Then, we deduce the fill factor and the current–voltage relation of the cell using detailed-balance analysis.[27] We first consider the detailed balance at the open-circuit voltage condition:

$$F_g = R_{\text{Aug}}(V_{\text{OC}}) + R(V_{\text{OC}}) \tag{6}$$

where F_g is the total carrier generation rate and R_{Aug} is the Auger recombination rate. R represents the combined effect of the radiative and surface recombinations. We already know F_g from carrier generation rate calculations (eq 2 and Figure 2). $R_{\text{Aug}}(V)$ can be expressed explicitly:[28−30]

$$R_{\text{Aug}}(V) = (C_n + C_p) W n_i^3 \exp\left(\frac{3qV}{2kT}\right) \tag{7}$$

where n_i is the intrinsic carrier concentration, C_n (C_p) is the conduction-band (valence-band) Auger coefficient, and W is the equivalent thickness of the solar cell. For T = 300 K, C_n and

DOI: 10.1021/acsphotonics.5b00081
ACS Photonics 2015, 2, 883–889

C_p are 2.8×10^{-31} and 0.99×10^{-31} cm^6 s^{-1}, respectively.[31] Here, we assume that $R(V)$ has the form

$$R(V) = C \exp\left(\frac{qV}{kT}\right) \tag{8}$$

where C is merely a constant. Having also computed V_{OC} using eq 1, we can calculate $R(V_{OC})$, and thus the constant C. This enables us to work out the current−voltage relation:

$$I/q = F_g - R_{Aug}(V) - R(V) \tag{9}$$

where V is the voltage across the cell and I is the current generated by the cell. From the current−voltage relation, we can find out the short-circuit current and the fill factor, which vary for different surface recombination velocities.

We use the procedure as outlined above to consider the limiting performance of the solar cell structure shown in Figure 1. The absorption properties of these structures, i.e., their photocurrent values, have already been discussed in detail in ref 16. Thus, here we mainly focus on the behaviors of the voltage and the efficiency. We examine two main factors influencing the open-circuit voltage and the efficiency: film thickness and surface recombination.

To study the effect of film thickness, we consider three films with different thicknesses: 1, 2, and 3 μm. For each thickness, the nanocone geometry is optimized in order to maximize light absorption as described by Wang et al.[16] Perfect surface passivation on both surfaces of the film is assumed in these simulations. Figure 4 illustrates the dependence of the open-circuit voltage on the thickness. The open-circuit voltage increases as the film thickness decreases. Qualitatively, reducing the film thickness leads to a higher concentration of carriers and hence a bigger split in quasi Fermi levels and, therefore, a higher open-circuit voltage.

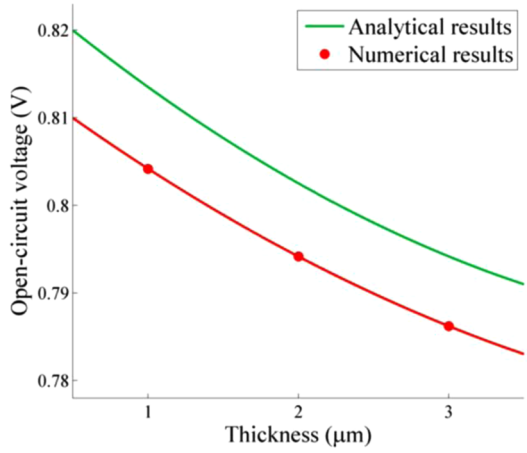

Figure 4. Open-circuit voltage as a function of the equivalent thickness of the cell obtained by the analytic model (green line) and the numerical model (red line with simulation results marked with dots). The physical thicknesses of the three structures considered are 1.362, 2.776, and 3.849 μm.

For the three structures shown in Figure 4, we now consider the effect of surface recombination on each of these structures, as shown in Figure 5. For all three structures, the open-circuit voltage decreases significantly as the surface recombination velocity increases, consistent with previous works, which have pointed out surface recombination as the main loss reason in the thin silicon solar cells.[10,32] Texturing enhances the surface area to volume ratio, which then boosts the surface recombination by increasing the probability of diffusing carriers hitting the surfaces and therefore recombining.[31]

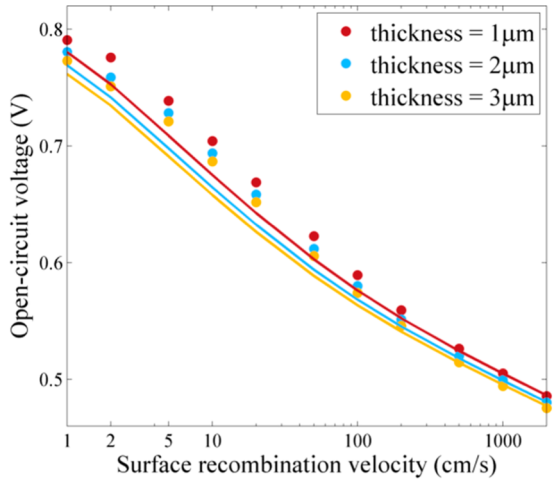

Figure 5. Open-circuit voltage as a function of surface recombination velocity obtained by the analytic model (solid line) and the simulations (dots) for three different cell thicknesses. Same surface recombination is assumed on both front and back surfaces.

We finally determine the fill factor and the energy conversion efficiency using the detailed-balance analysis as described above. Since the detailed-balance analysis is used to deduce the fill factor, parasitic resistance losses due to series resistance and shunt resistance are ignored. However, the adverse effect of the surface recombination is still reflected on the fill factor. For the surface recombination velocities between 0 and 2000 cm/s, the fill factor ranges from 0.87 to 0.79. Having the short-circuit current, the open-circuit voltage, and the fill factor calculated, we find an energy conversion efficiency of 24.9% achievable with a 3 μm thick solar cell assuming perfect surface passivation. The presence of surface recombination causes sharp falls in the efficiency (Figure 6). However, a moderate surface passivation with surface recombination velocities around 20 cm/s is still sufficient to obtain efficiencies above 20%. Thus, our theoretical analysis indicates that such an ultrathin silicon cell has significant potential for achieving high

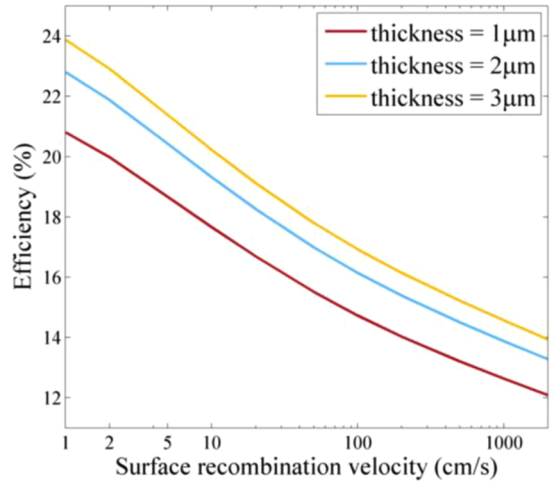

Figure 6. Energy conversion efficiency as a function of surface recombination velocity for three cells with different thicknesses.

DOI: 10.1021/acsphotonics.5b00081
ACS Photonics 2015, 2, 883−889

efficiency. Moreover, the efficiency of the cell for all three thicknesses ranging from 1 to 3 μm will drop by several percentage points when the surface recombination velocity increases from 1 to 5 cm/s, highlighting the great importance of surface recombination in these ultrathin cells.

The analysis above requires a detailed three-dimensional electronic simulation. Below, we show that the main results of the electronic simulations of the solar cell can instead be accounted for with an analytic model. As a result, we can obtain the optoelectronic properties of the cell by combining the results of the optical simulations with such an analytic model for the electronic properties, which significantly simplifies the overall analysis.

This simplified analysis also uses eq 1 to determine the open-circuit voltage. The carrier concentration required in eq 1 is determined by the balance between carrier generation and recombination rates. Since the resulting carrier concentration is spatially uniform, as we see in the simulation, only the spatially averaged values of generation and recombination rate is important. Therefore, we average the generation rate profile obtained by optical simulations. The recombination rate is also represented by a single effective lifetime for the excess minority carrier:

$$\text{Recombination} = \frac{\Delta n}{\tau_{\text{eff}}} \tag{10}$$

We note that in general τ_{eff} is a function of Δn and can be expressed in terms of bulk and surface recombination lifetimes as

$$\frac{1}{\tau_{\text{eff}}} = \frac{1}{\tau_{\text{bulk}}} + \frac{1}{\tau_{\text{surface}}} \tag{11}$$

For bulk recombination lifetime τ_{bulk}, we use the analytic formula given by eq 4, where Auger recombination and radiative recombination are accounted for.[22] Determining the surface recombination lifetime τ_{surface} necessitates analysis of the effects of the texture. For flat cells, the surface recombination lifetime is expressed in terms of surface recombination velocities.[33−35]

$$\frac{1}{\tau_{\text{surface}}} = \alpha^2 D \tag{12}$$

Here, D is the diffusion constant. Its dependency on the carrier concentration can be determined using an ambipolar diffusion model.[36] α is the smallest positive root of the equation:

$$\tan(\alpha W) = \frac{S_{\text{front}} + S_{\text{back}}}{\alpha D - \frac{S_{\text{front}} S_{\text{back}}}{\alpha D}} \tag{13}$$

where S_{front} and S_{back} are the front and back surface recombination velocities, respectively, and W is the cell thickness. To calculate τ_{surface} for the textured cell, as a simple approach, we use the same eqs 9 and 10, but we make two modifications. First, for textured cells we take W as the equivalent thickness. Second, since for the same equivalent thickness the textured cell has a larger surface area, S_{front} and S_{back} are scaled as much as the area enhancement due to texturing on the respective surface.[37] Such a modification is justified from the uniformity of the steady-state carrier distribution: If the carriers' distribution is uniform, we would expect the surface recombination loss to scale linearly with respect to the surface area.

The approach as outlined above results in an analytic (and nonlinear) relation between the recombination rate and the carrier concentration. Balancing the recombination with the generation rate thus results in an equation that can be solved self-consistently to obtain Δn and, hence, the open-circuit voltage through eq 1.

The analytic model based upon the simplifying assumptions above is validated against the numerical simulations for the three structures with equivalent thicknesses ranging from 1 to 3 μm, as shown in Figure 4. The analytic model very nicely accounts for the overall trend in the numerical analysis. The analytic model predicts a strong dependence of the open-circuit voltage on the thickness. Such a dependency has been pointed out in the Tiedje−Yablonovitch's model on silicon solar cells' limiting efficiency for conventional solar cells.[30] Here we show that the same dependency also holds for ultrathin cells. The analytic model also quantitatively accounts for the strong dependency of the open-circuit voltage on the surface recombination velocity, as shown in Figure 5.

The discrepancy in open-circuit voltage between the analytic model and the numerical results is within 4%. Since the analytic model used here does not require three-dimensional electronic simulations, and also given the wide availability of the three-dimensional optical simulation software, we believe such an analytic model can play a significant role in understanding and designing nanostructured crystalline silicon cells.

Finally, we introduce (defect-assisted) Shockley−Read−Hall recombination in our model. As previously discussed, for the c-Si nanostructured solar cells operating in the high-injection regime, SRH recombination is negligible compared to Auger and surface recombinations. Moreover, previous studies showed that the defects causing SRH recombination in c-Si could be almost completely eliminated with processing techniques.[38,39] For experimental solar cell structures, record bulk lifetimes as high as 32 ms were achieved.[40] For commercially available c-Si cells, some of the high-quality cells have bulk lifetimes ranging from 1 to 5 ms.[41] Being a portion of the bulk lifetime, SRH lifetimes would be higher than the reported bulk lifetimes. In our model, we treat SRH recombination as an additional recombination process characterized by a recombination lifetime τ_{SRH}, ranging from 5×10^{-3} to 2 ms. In Figures 7

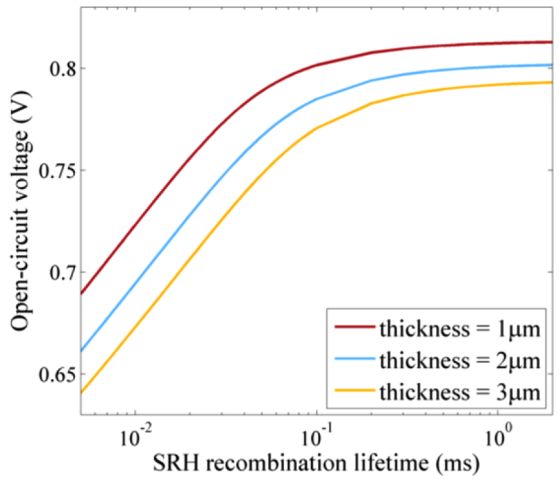

Figure 7. Open-circuit voltage as a function SRH recombination lifetime obtained by the analytic model when surface recombination is assumed to be zero.

DOI: 10.1021/acsphotonics.5b00081
ACS Photonics 2015, 2, 883−889

and 8, we plot the open-circuit voltage and the cell efficiency as a function of τ_{SRH}. The results demonstrated in Figures 7 and 8

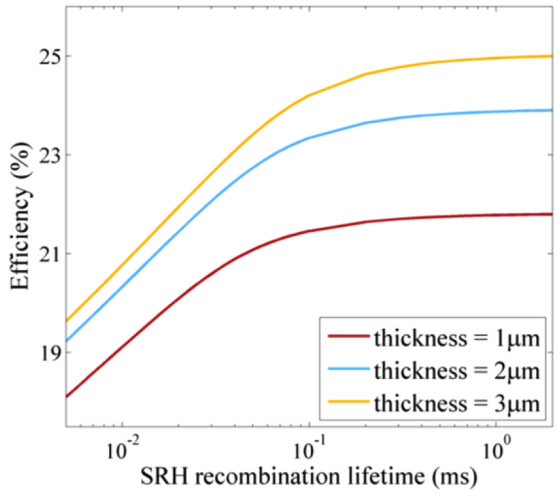

Figure 8. Energy conversion efficiency as a function SRH recombination lifetime obtained by the analytic model when surface recombination is assumed to be zero.

show that for a SRH lifetime higher than 0.1 ms SRH recombination becomes negligible. This corresponds to a lifetime that is an order of magnitude less than the already achieved high SRH lifetimes in high-quality commercial solar cells. For that reason, we conclude that it is safe to assume that SRH recombination is negligible in nanostructured ultrathin c-Si solar cells.

In conclusion, we have presented a coupled optoelectrical analysis of nanostructured crystalline silicon cells. Our analysis illustrates the intrinsic dependence of the performance of these cells on the fundamental recombination processes. The analysis in particular quantifies the importance of surface passivation on the behaviors of the solar cells. On the basis of the results of the numerical simulations, we also propose an analytic model that accurately captures the main physics and significantly simplifies the otherwise computationally expensive analysis of these solar cells.

AUTHOR INFORMATION

Corresponding Author

*E-mail: shanhui@stanford.edu.

Notes

The authors declare no competing financial interest.

ACKNOWLEDGMENTS

This work is supported by the Bay Area Photovoltaic Consortium (BAPVC) funded under the Sunshot Initiative of the U.S. Department of Energy (I.K.) and by the Department of Energy Grant No. DE-FG07ER46426 (K.W.). I.K. also acknowledges support from the Fulbright Science and Technology Fellowship by the Institute of International Education.

REFERENCES

(1) Park, Y.; Drouard, E.; El Daif, O.; Letartre, X.; Viktorovitch, P.; Fave, A.; Kaminski, A.; Lemiti, M.; Seassal, C. Absorption enhancement using photonic crystals for silicon thin film solar cells. *Opt. Express* **2009**, *17*, 14312−14321.

(2) Sheng, X.; Johnson, S. G.; Michel, J.; Kimerliing, L. C. Optimization-based design of surface textures for thin-film Si solar cells. *Opt. Express* **2011**, *19*, A841.

(3) Gjessing, J.; Sudbo, A. S.; Marstein, E. S. Comparison of periodic light-trapping structures in thin crystaline silicon solar cells. *J. Appl. Phys.* **2011**, *110*, 033104.

(4) Biswas, R.; Xu, C. Nano-crystalline silicon solar cell architecture with absorption at the classical 4n2 limit. *Opt. Express* **2011**, *19*, A664.

(5) Fahr, S.; Kirchartz, T.; Rockstuhl, C.; Lederer, F. Approaching the Lambertian limit in randomly textured thin-film solar cells. *Opt. Express* **2011**, *19*, A865.

(6) Zhang, R. Y.; Shao, B.; Dong, J. R.; Zhang, J. C.; Yang, H. Absorption enhancement analysis of crystalline Si thin film solar cells based on broadband antireflection nanocone grating. *J. Appl. Phys.* **2011**, *110*, 113105.

(7) Meng, X.; Drouard, E.; Gomard, G.; Peretti, R.; Fave, A.; Seassal, C. Combined front and back diffraction gratings for broad band light trapping in thin film solar cell. *Opt. Express* **2012**, *20*, A560−A571.

(8) Deceglie, M. G.; Ferry, V. E.; Alivisatos, A. P.; Atwater, H. A. Design of nanostructured solar cells using coupled optical and electrical modeling. *Nano Lett.* **2012**, *12*, 2894−2900.

(9) Meng, X.; Depauw, V.; Gomard, G.; El Daif, O.; Trompoukis, C.; Drouard, E.; Jamois, C.; Fave, A.; Dross, F.; Gordon, I.; Seassal, C. Design, fabrication and optical characterization of photonic crystal assisted thin film monocrystalline-silicon solar cells. *Opt. Express* **2012**, *20*, A465−A475.

(10) Jeong, S.; McGehee, M. D.; Cui, Y. All-back-contact ultra-thin silicon nanocone solar cells with 13.7% power conversion efficiency. *Nat. Commun.* **2013**, *4*, 2950.

(11) Deinega, A.; Eyderman, S.; John, S. Coupled optical and electrical modeling of solar cell based on conical pore silicon photonic crystals. *J. Appl. Phys.* **2013**, *113*, 224501.

(12) Hara, K. O.; Usami, N. Theory of open-circuit voltage and the driving force of charge separation in pn-junction solar cells. *J. Appl. Phys.* **2013**, *114*, 153101.

(13) Green, M. A. Generalized relationship between dark carrier distribution and photocarrier collection in solar cells. *J. Appl. Phys.* **1997**, *81*, 268−271.

(14) Sinton, R. A.; Cuevas, A. Contactless determination of current−voltage characteristics and minority carrier lifetimes in semiconductors from quasisteadystate photoconductance data. *Appl. Phys. Lett.* **1996**, *69*, 2510.

(15) Schuster, C. S.; Bozzola, A.; Andreani, L. C.; Krauss, T. F. How to access light trapping structures versus a Lambertian scatterer for solar cells. *Opt. Express* **2014**, *22*, A542−A551.

(16) Wang, K. X.; Yu, Z.; Cui, Y.; Fan, S. Absorption enhancement in ultrathin crystalline silicon solar cells with antireflection and light-trapping nanocone gratings. *Nano Lett.* **2012**, *12*, 1616−1619.

(17) Li, L. New formulation of the Fourier modal method for crossed surface-relief gratings. *J. Opt. Soc. Am. A* **1997**, *14*, 2758−2767.

(18) Tikhodeev, S. G.; Yablonskii, A. L.; Muljarov, E. A.; Gippius, N. A.; Ishihara, T. Quasiguided modes and optical properties of photonic crystal slabs. *Phys. Rev. B* **2002**, *66*, 045102.

(19) Liu, V.; Fan, S. S4: A free electromagnetic solver for layered periodic structures. *Comput. Phys. Commun.* **2012**, *183*, 2233−2244.

(20) *Handbook of Optical Constants of Solids*; Palik, E. D., Ed.; Academic Press: New York, 1985.

(21) *Sentaurus, TCAD*, Z-2012.03 ed.; Synopsys. Inc., 2012.

(22) Kerr, M. J.; Cuevas, A. General parameterization of Auger recombination in crystalline silicon. *J. Appl. Phys.* **2002**, *91*, 2473.

(23) Sinton, R. A.; Swanson, R. M. Recombination in highly injected silicon. *IEEE Trans. Electron Devices* **1987**, *34*, 1380−1389.

(24) Yablonovitch, E.; Gmitter, T. Auger recombination in silicon at low carrier densities. *Appl. Phys. Lett.* **1986**, *49*, 587.

(25) Schmidt, J.; Veith, B.; Brendel, R. Effective surface passivation of crystalline silicon using ultrathin Al_2O_3 films and Al_2O_3/SiNx stacks. *Phys. Status Solidi RRL* **2009**, *3*, 287−289.

DOI: 10.1021/acsphotonics.5b00081
ACS Photonics 2015, 2, 883−889

(26) Dingemans, G.; Kessels, W. M. M. Status and prospects of Al_2O_3-based surface passivation schemes for silicon solar cells. *J. Vac. Sci. Technol. A* **2012**, *30*, 040802.
(27) Shockley, W.; Queisser, H. J. J. Detailed balance limit of efficiency of pn junction solar cells. *Appl. Phys.* **1961**, *32*, 510−519.
(28) Miller, O. D.; Yablonovitch, E.; Kurtz, S. R. Strong internal and external luminescence as solar cells approach the Shockley−Queisser limit. *IEEE J. Photovoltaics* **2012**, *2*, 303−311.
(29) Green, M. A. Limits on the open-circuit voltage and efficiency of silicon solar cells imposed by intrinsic Auger processes. *IEEE Trans. Electron Devices* **1984**, *31*, 671−678.
(30) Tiedje, T.; Yablonovitch, E.; Cody, G. D.; Brooks, B. G. Limiting efficiency of silicon solar cells. *IEEE Trans. Electron Devices* **1984**, *31*, 711−716.
(31) Pierret, R. F. *Semiconductor Fundamentals*, 2nd ed.; Prentice Hall: Upper Saddle River, NJ, 1988; Vol. *1*, Chapter 2, pp 27−31.
(32) Green, M. A. Limiting efficiency of bulk and thin-film silicon solar cells in the presence of surface recombination. *Prog. Photovoltaics: Res. Appl.* **1999**, *7*, 327−330.
(33) Luke, K. L.; Cheng, L. Analysis of the interaction of a laser pulse with a silicon wafer: Determination of bulk lifetime and surface recombination velocity. *J. Appl. Phys.* **1987**, *61*, 2282−2293.
(34) Otaredian, T. Separate contactless measurement of the bulk lifetime and the surface recombination velocity by the harmonic optical generation of the excess carriers. *Solid-State Electron.* **1993**, *36*, 153−162.
(35) Sproul, A. B. Dimensionless solution of the equation describing the effect of surface recombination on carrier decay in semiconductors. *J. Appl. Phys.* **1994**, *76*, 2851−2854.
(36) Rosling, M.; Bleichner, H.; Jonsson, P.; Nordlander, E. The ambipolar diffusion coefficient in silicon: Dependence on excess-carrier concentration and temperature. *J. Appl. Phys.* **1994**, *76*, 2855−2859.
(37) Xiong, K.; Lu, S.; Jiang, D.; Dong, J.; Yang, H. Effective recombination velocity of textured surfaces. *Appl. Phys. Lett.* **2010**, *96*, 193107.
(38) Ciszek, T. F.; Wang, T.; Schuyler, T.; Rohatgi, A. Some effects of crystal growth parameters on minority carrier lifetime in float-zoned silicon. *J. Electrochem. Soc.* **1989**, *136*, 230−234.
(39) Ciszek, T. F.; Wang, T. H. *Silicon defect and impurity studies using controlled samples*; Proceedings of the 14th European Photovoltaic Solar Energy Conference, 1997; pp 396−399.
(40) Kerr, M. J.; Cuevas, A. Very low bulk and surface recombination in oxidized silicon wafers. *Semicond. Sci. Technol.* **2002**, *17*, 35−38.
(41) Smith, D. D.; et al. *Generation III high efficiency lower cost technology: Transition to full scale manufacturing*. IEEE Photovoltaic Specialists Conference, 2012; pp 1594−1597.

DOI: 10.1021/acsphotonics.5b00081
ACS Photonics 2015, 2, 883−889